*Original Article*

JCBFM

Journal of Cerebral Blood Flow & Metabolism
2023, Vol. 43(6) 905–920

DOI: 10.1177/0271678X231152551
journals.sagepub.com/home/jcbfm
Sage

# Xanthine oxidase mediates chronic stress-induced cerebrovascular dysfunction and cognitive impairment

**Emily N Burrage[1], Tyler Coblentz[2], Saina S Prabhu[3], Ryan Childers[2], Randy W Bryner[2], Sarah E Lewis[4], Evan DeVallance[4], Eric E Kelley[4] and Paul D Chantler[1,2]**

## Abstract

Xanthine oxidase (XO) mediates vascular function. Chronic stress impairs cerebrovascular function and increases the risk of stroke and cognitive decline. Our study determined the role of XO on stress-induced cerebrovascular dysfunction and cognitive decline. We measured middle cerebral artery (MCA) function, free radical formation, and working memory in 6-month-old C57BL/6 mice who underwent 8 weeks of control conditions or unpredictable chronic mild stress (UCMS) with or without febuxostat (50 mg/L), a XO inhibitor. UCMS mice had an impaired MCA dilation to acetylcholine vs. controls ($p < 0.0001$), and increased total free radical formation, XOR protein levels, and hydrogen peroxide production in the liver compared to controls. UCMS increased hydrogen peroxide production in the brain and cerebrovasculature compared to controls. Working memory, using the y-maze test, was impaired ($p < 0.05$) in UCMS mice compared to control mice. However, blocking XO using febuxostat prevented the UCMS-induced impaired MCA response, while free radical production and hydrogen peroxide levels were similar to controls in the liver and brain of UCMS mice treated with febuxostat. Further, UCMS + Feb mice did not have a significant reduction in working memory. These data suggest that the cerebrovascular dysfunction associated with chronic stress may be driven by XO, which leads to a reduction in working memory.

## Keywords

Cerebrovasculature, chronic stress, cognitive impairment, endothelial function, xanthine oxidase, middle cerebral artery, nitric oxide

Received 29 July 2022; Revised 19 December 2022; Accepted 3 January 2023

## Introduction

Chronic psychological stress is a major global health-related burden.[1] Seventy-five percent of Americans report experiencing psychological stress with 28% of these individuals reporting that stress has a negative impact on their mental health, and 25% reporting a negative impact on their physical health.[2,3] In fact, chronic stress has been identified as a powerful risk factor in the development of various cerebrovascular diseases such as stroke and dementia,[4,5] which are the leading cause of long-term disability, and the second leading cause of death worldwide,[6] establishing chronic stress as a leading disease burden.

We have previously shown that chronic stress in rats induces significant cerebrovascular dysfunction as well as produces a substantial pro-oxidative environment.[7,8] However, the source of this pro-oxidative environment leading to cerebrovascular dysfunction with chronic stress is unknown. An increase in the xanthine

[1]Department of Neuroscience, West Virginia University School of Medicine, Morgantown, WV, USA
[2]Division of Exercise Physiology, West Virginia University School of Medicine, Morgantown, WV, USA
[3]Department of Pharmaceutical Sciences, West Virginia University School of Medicine, Morgantown, WV, USA
[4]Department of Physiology and Pharmacology, West Virginia University School of Medicine, Morgantown, WV, USA

**Corresponding author:**
Paul D Chantler, 64 Medical Center Drive, Morgantown, WV 26505, USA.
Email: pchantler@hsc.wvu.edu

oxidase (XO) has been identified in the plasma and post-mortem brain tissue of stress/depressed patients.[9,10] And in a pre-clinical model, Yisieyili et al.[11] noted an increase in oxidative stress alongside increased XO activity in the liver, visceral adipose tissue, and intestines of mice exposed to restraint stress. Others have shown the importance of the XO pathway in inducing arterial dysfunction in the context of hypertension,[12] sickle cell disease,[13] and diabetes.[14] However, the role of XO in psychological stress-induced cerebrovascular dysfunction and cognitive decline has yet to be established.

Xanthine oxidoreductase (XOR) oxidizes hypoxanthine to xanthine and xanthine to uric acid and exists in two forms: xanthine dehydrogenase (XDH) and xanthine oxidase (XO).[15,16] While XDH utilizes $NAD^+$ as an electron acceptor, XO donates electrons to molecular oxygen resulting in the production of superoxide anions and hydrogen peroxide, and is most abundant during proinflammatory processes including chronic stress.[15,16] XDH is transcribed and translated with the greatest specific activity observed in the liver; however, following hepatic stressors, such as inflammation, hypoxia, or ischemia, XDH can be released from hepatocytes to the circulation where it is rapidly converted to XO by plasma proteases.[17,18] XO has a high affinity for glycosaminoglycans (GAGs) on the vascular endothelium, where its immobilization on the endothelial surface places it, in a prime position to induce endothelial dysfunction via oxidant production.[19] As it is well-established that chronic stress induces cerebrovascular dysfunction via an increase in oxidative stress[7] and chronic stress has been noted to increase oxidative stress through XO activity,[11] it is important to explore the role of XO mediating the cerebrovascular dysfunction noted with chronic stress. Therefore, we hypothesize that XO inhibition would prevent cerebrovascular dysfunction and cognitive impairment noted with chronic stress (unpredictable chronic mild stress (UCMS) paradigm).

## Methods

### Animals

Male and female C57BL/6J mice (stock no. 000664) were obtained from The Jackson Laboratory (Bar Harbor, ME) at 15–16 weeks of age and they were allowed to acclimate to the new environment for at least a week. At 18 weeks of age, all animals were singly-housed and randomly assigned to one of the following groups for 8 weeks: 1) control (i.e., non-UCMS, Con), 2) UCMS, 3) control+febuxostat, (Con + Feb) 4) UCMS + febuxostat (UCMS + Feb). Once on protocol, all mice were handled daily and moved into a new room with UCMS mice undergoing the chronic stress paradigm and control mice being placed on a static rack, allowing all mice to have similar exposure to experimenter intervention. All animals were fed standard chow and tap water ad libitum for all experiments. Protocols received prior approval from the WVU HSC Animal Care and Use Committee as per the National Institutes of Health Office of Laboratory Animal Welfare guidelines. All experiments were reported in accordance with the ARRIVE (Animal Research: Reporting in vivo Experiments) guidelines[20] A total of 147 male/female C57BL/6J mice aged 15–16 weeks were used in this study.

### Febuxostat treatment

Vehicle (standard drinking water) or febuxostat (Axon Medchem BV, Netherlands) was delivered daily in the drinking water at a concentration of 50 mg/L. The water was measured frequently to calculate the concentration of drug consumed daily (~5–6 mg/kg per day) which was shown to effectively inhibit XO.[21]

### UCMS protocol

Previous investigators developed the UCMS paradigm to elicit a chronic stress phenotype in rodents.[22] The UCMS model is considered to be the most appropriate rodent model to elicit a chronic stress phenotype, based on its ability to reproduce anxiety-like behaviors as well as its ability to lead to the development of symptoms related to the clinical consequences of chronic stress such as anhedonia, learned helplessness, and memory impairment.[7,23–25] Our lab has successfully utilized this paradigm to elicit chronic stress-induced vascular alterations.[7,24,26]

In UCMS groups, mice were exposed to the following mild environmental stressors in randomly chosen sequences for 7 hours each day, 5 days/week, over the course of 8 weeks:

1. *Damp bedding* – 10 oz. of water was added to each standard cage
2. *Bath* – all bedding was removed and ~0.5 inches of water was added to the empty cage. The water temperature was room temperature, ~24 °C
3. *Cage Tilt* – cage was tilted to 45 degrees without bedding
4. *Social stress* – each mouse was switched into a cage of a neighboring mouse
5. *No bedding* – all bedding was removed from the cage
6. *Alteration of light/dark cycles* –turning lights off/on in random increments for a scheduled period.

## Stress markers

At the time of death, plasma was collected, and corticosterone levels were examined in triplicate according to the manufacturer's instructions (ELISA kit: Arbor Assay, Item #K014). During the duration of the 8-week protocol, the rodent's coats were evaluated. Each week the mice were inspected for grooming habits;[27] the total cumulative coat score was computed by giving an individual score of 0 (clean) or 1 (dirty) to eight different body parts (e.g. head, neck, back, forelimbs, stomach, hindlimbs, tail, genitals). Following the 8-week protocol, sucrose splash testing was performed to assess grooming behavior. The sucrose splash test consisted of spraying a 10% sucrose solution on the dorsal coat of a mouse in an empty cage; latency to begin grooming as well as frequency were recorded for a total of 5 minutes.[28]

## Behavior

*Y-maze spontaneous alternation test.* Following a 30-minute room acclimation period under indirect dim illumination conditions (approximately 150 lx), short-term working memory was assessed. Mice were placed in the three-armed, Y-shaped apparatus (approximate arm length = 38 cm, width = 8.25 cm, height = 13.25 cm) and allowed to freely explore for 8 min. Movement in the apparatus was recorded using the Anymaze tracking software (Stoelting, Chicago, IL). The innate tendency of mice to spontaneously alternate between the three arms and enter the least recently visited arm was assessed by determining the percentage of successful alternations ((number of correct alternations/(total arm entries − 2) * 100). Other dependent variables recorded included distance moved (m) and speed (m/s). The apparatus was cleaned of debris and olfactory cues between each animal using an anti-bacterial disinfectant (Virkon, Pharmacol, CT).

*Open field test.* In this task, total movement in the area indicates general locomotor ability.[29] The apparatus consisted of a clear plastic box (40 cm × 40 cm) surrounded by a 16 × 16 laser beam array (San Diego Instruments, CA) that allowed for the assessment of movement in the horizontal axis. A second array placed 3.8 cm above the first beam allowed for the assessment of locomotion in the vertical axis (rearing behavior). Following a 30-minute acclimation to the testing room (approximately 1500 lx), each mouse was placed in the center point of the arena and allowed to freely explore for 30 min. Total horizontal movements via beam breaks in the arena and the number of vertical beam breaks (rearing) were recorded. The 30-minute phase was also broken down into 6 five-minute intervals, which when analyzed individually did not reveal any differences.

*Vascular reactivity/mechanics.* Mice were euthanized, and the brain was carefully removed from the skull and placed in cold physiological salt solution (PSS; 4 °C). Both middle cerebral arteries (MCA), which supply ≈50% of the cerebral blood flow,[30] were dissected from their origin at the Circle of Willis and placed into an isolated microvessel chamber (living systems) filled with PSS. Each MCA was subsequently doubly cannulated within a heated chamber (37 °C) that allowed the lumen and exterior of the vessel to be perfused and superfused, respectively, with PSS from separate reservoirs. The PSS was equilibrated with a 21% $O_2$, 5% $CO_2$, and 74% $N_2$ gas mixture and had the following composition (mM): 119 NaCl, 4.7 KCl, 1.17 $MgSO_4$, 1.6 $CaCl_2$, 1.18 $NaH_2PO_4$, 24 $NaHCO_3$, 0.026 EDTA, and 5.5 glucose. Any side branches were ligated. MCA diameter was measured using television microscopy and an on-screen video micrometer.

*Measurements of vascular reactivity in isolated MCA.* Following cannulation, MCAs were extended to their in-situ length and were equilibrated at 70 mmHg mean arterial pressure. Active tone at the equilibration pressure was calculated as (ΔD/Dmax) × 100, where ΔD is the diameter increase from rest in response to $Ca^{2+}$-free PSS, and Dmax is the maximum diameter measured at the equilibration pressure in $Ca^{2+}$-free PSS. Following equilibration, the MCA dilator reactivity was assessed in response to increasing concentrations of acetylcholine (ACh, $10^{-9}$ M–$10^{-4}$ M) to reflect endothelial-dependent dilation (EDD), and increasing concentrations of sodium nitroprusside (SNP $10^{-9}$ M–$10^{-4}$ M) to reflect endothelial independent dilation (EID), and a potent vasoconstrictor (phenylephrine, PE $10^{-9}$ M–$10^{-4}$ M). To assess the effects of NO on EDD, the MCA was acutely incubated (30 minutes) with L-NAME ($10^{-4}$ M) and the MCA EDD response to ACh was repeated. To assess the acute effects of oxidative stress on modulating EDD, we acutely (30 minutes) incubated the MCA with: 1) XO (40 uM; purified from Kelley lab as previously published[31]) supplemented with xanthine (10 uM, Sigma Aldrich, cat# X2502); 2) TEMPOL ($10^{-4}$ M, Sigma Aldrich, cat# 176141); and 3) febuxostat (10 mM; Axon Medchem BV, Netherlands). Following completion of all procedures, the perfusate and superfusate were replaced with $Ca^{2+}$-free PSS and the passive diameter of the fully relaxed MCA was determined over an intralumenal pressure range of 5–140 mmHg at 20-mmHg pressure increments. After 7 min at each intraluminal pressure, the inner and outer diameters of the passive MCA were determined. Media thickness, lumen and outer diameters, and vessel cross-sectional

areas (used as indicators of structural alterations to the individual microvessel) were determined as follows: Media thickness (WT, μm) = Outer diameter – lumen diameter (i.e., OD – LD); media-to-lumen (M:L) ratio = MT/LD; Cross-sectional area ($\mu m^2$) = Outer vessel area – lumen area. Myogenic tone was assessed using the following formula: 1-(active diameter/passive diameter)*100 (Rigsby, 2007). NO-dependent dilation was determined from the maximal EDD in the absence or presence of L-NAME according to the following formula: NO-dependent dilation (μm) = Maximum $\text{dilation}_{\text{ACh}}$ − Maximum $\text{dilation}_{\text{ACh+L-NAME}}$.

*Cerebral microvessel isolation.* To explore the vascular signaling pathway, the mouse brain was carefully removed, the MCA was dissected for pressure myography, and then the remaining cerebral microvessels (parenchymal and meninges vessels) were isolated from the brain using the dextran centrifugation method. In brief, brain tissue was homogenized in 1X PBS and centrifuged at 2960 rpm at 4 °C. The supernatant, containing parenchymal tissue was discarded; the pellet was resuspended and layered over 15% Dextran (in 1X PBS) (Sigma Aldrich, Item #31390). Following a 30-minute centrifugation at 4000 rpm at 4 °C, the supernatant was discarded, and the pellet was resuspended in 1% bovine serum albumin (BSA) in 1X PBS. The suspension was then passed through a 70um cell strainer with the microvessels being collected on the mesh. The microvessels were then washed with 1% BSA in 1X PBS and collected by centrifugation at 3000 rpm for 10 min at 4 °C. Following this, microvessels were rinsed with 1X PBS, centrifugated at 4000 rpm for 5 min at 4 °C, and flash frozen for future use in other assays (adapted from[32]).

*Tissue oxidants.* As briefly described below, the brain, liver, and microvessels were explored for oxidative products. Tissue samples were dissected, flash froze in liquid nitrogen, and stored at −80 °C until analysis.

*Xanthine oxidase-HPLC.* Plasma, liver, and brain tissue XO activity was measured as previously described using high-performance liquid chromatography (HPLC).[13,21] Frozen samples were homogenized in ice-cold RIPA containing a protease inhibitor cocktail (Sigma) and briefly spun down. Tissue samples were processed as described below with a sample volume of 10 μL. Uricase was inhibited by oxonic acid (100 μM) to avoid an underestimation of enzyme activity. Total XOR activity was determined on the basis of the rate of uric acid production in the presence of xanthine (75 μM) and nicotinamide adenine dinucleotide (NAD+, 0.5 mM; for tissue samples only). Allopurinol (100 μM), an inhibitor of XOR, was used in parallel samples to confirm that urate formation was specific. After 60 min of incubation at 37 °C, the reaction was terminated by protein precipitation with cold acetonitrile. The samples were then centrifuged for 12 min at 11,900 rpm, at 4 °C. Following centrifugation, the supernatant was removed and placed in borosilicate glass tubes. After a 60-minute dry-down process, the samples were resuspended in the isocratic mobile phase (300 μL) and filtered through a 0.20 μm nylon membrane filter unit into an 11 mm plastic snap top auto-sampler vials. The uric acid content of protein-free samples was determined by an HPLC-based electrochemical technique as described below. One unit of activity (U) is defined as 1 μmole/min urate formed at 37 °C and pH 7.4. Total protein concentration was determined by the bicinchoninic acid method (BCA, Pierce). Measurements were carried out blindly without knowledge by the operator of the animal treatment groups. Uric acid was measured by electrochemical detection (Vanquish UltiMate 3000 ECD-3000RS) coupled to reverse-phase HPLC using a Phenomenex column (Luna 3 μm C18(2) 100 A, 150 × 4.6 mm) and isocratic mobile phase (50 mM sodium dihydrogen phosphate, 4 mM dodecyltrimethylammonium chloride, 2.5% methanol, pH 7.0). Potentials for 3 channels were as follows: −100 mV, 30 mV, and 390 mV. Quantitation/integration was performed on the dominant peak. In the case of XO activity in plasma, 10–20 μL of plasma was used in lieu of tissue and processed with the same protocol as above. XO activity in plasma utilized volume (U/mL) as a denominator rather than protein.

*Xanthine oxidase-Western blots.* Liver and brain tissue was homogenized in 1X PBS plus HALT inhibitor and then centrifuged at 3000 rpm at 4 °C for 20 min. Equal amounts of protein for each sample were loaded into a polyacrylamide gel. After the completion of gel electrophoresis, the protein was transferred to nitrocellulose membranes overnight. XO expression was assessed using a xanthine oxidase antibody (1:500; Santa Cruz; cat # sc-398548) followed by a secondary antibody (1:10,000; Licor; cat # 925-32201 and 925-68071). GAPDH (1:1000; Cell Signaling; cat #2118) was used as a loading control. Blots were imaged using Licor Odyssey and band intensity was assessed using ImageJ software.

*Coumarin boronic acid (CBA) assay.* Hydrogen peroxide ($H_2O_2$) abundance was measured in homogenate from the liver, brain, and brain microvessel using the CBA (Cayman #14051) assay adapted from Zielonka et. al[33] as previously described.[26,34] In brief, 10 μg of lysates were loaded, in triplicate, into wells of a 384-well black-sided clear bottom plate. Subsequently, assay buffer composed of HBSS supplemented with 25 mM

HEPES, 1% BSA, 10uM DTPA, 100uM l-NAME, and 1 mM Taurine was added and then CBA was added to each well at a final concentration of 0.5 mM. One well from each biological sample received an additional 1 KU/ml bovine liver catalase to act as a negative control. Upon addition of the CBA, plates were placed in a Biotek plate reader preheated to 37 °C and read kinetically at excitation 350 nm and emission 450 nm. The average rate of fluorescence was determined over the linear portion of the response and then normalized by subtracting out the rate of fluorescence from the negative control and taking the fold change from the control group.

*In vivo immuno-spin trapping.* In a separate cohort of mice (3/sex/group), an i.p injection of 5,5-Dimethyl-1-Pyrroline-N-Oxide (DMPO: 1.5 g/kg) in $3 \times 0.5$ g/kg doses was given at 24, 12, 6 hours prior to euthanasia, as previously reported.[35,36] Upon euthanization, organs/tissues were perfused with phosphate-buffered saline (PBS; pH 7.4), removed, frozen in liquid $N_2$, and stored at −80 °C for Western blot analysis. Liver and brain tissue were homogenized in RIPA buffer plus HALT inhibitor and then centrifuged at 3000 rpm at 4 °C for 20 min to remove insoluble materials. An equal amount of protein for each sample was loaded into a polyacrylamide gel. After the completion of gel electrophoresis, the protein was transferred to nitrocellulose membranes overnight. DMPO-adducted proteins were assessed using mouse anti-DMPO (1:500, Enzo Life Science, Item #ALX-803-340) followed by a secondary antibody (1:10,000; Licor; cat # 925-32201 and 925-68071). GAPDH (1:1000; Cell Signaling; cat #2118) was used as a loading control. Blots were imaged using Licor Odyssey and band intensity was assessed using ImageJ software.

*Statistics.* Power analysis was performed using PASS 15 software and based on preliminary data, the sample size was calculated based on the vascular outcomes and powered off max MCA EDD ($2 \times 4 \times 2$ factorial ANOVA, 99% power, $\alpha = 0.05$), a sample size of 8/sex/group (2 conditions: non-UMCS vs. UCMS; 4 groups: Con, Con + Feb, UCMS, UCMS + Feb; sex: male vs. female) would provide 99% power to find a significant difference in EDD among groups: however to ensure we had sufficient tissues to perform the microvessel isolation, the separation of brain tissue (for IHC, Western blots, and CBA), and the behavioral analysis we added a number of cohorts over the year. Further, as the in vivo immuno-spin trapping procedure requires the single use of a mouse, we had a separate cohort of mice (3/sex/group) for that procedure. Total mouse numbers/group are detailed in the figure legends. During data collection, groups were unknown to the experimenter. Data are presented as mean ± SD unless otherwise stated. Normality was evaluated by the Kolmogorov–Smirnov test. As no statistical differences were noted between male and female mice for all variables, male and female data were combined for statistical approaches. The MCA maximal reactivity, MCA remodeling, and molecular approaches were analyzed by a two-way (UCMS and Febuxostat) analysis of variance (ANOVA) with an interaction term, and a Tukey post-hoc test was performed to determine differences among groups. The clinical characteristics, behavioral tests, and the effects of TEMPOL, XO, acute febuxostat, and L-NAME on the maximal dilation of the MCA were examined with a two-way ANOVA or a repeated-measures ANOVA with an interaction term, and a Tukey post-hoc test was performed when appropriate. Data analysis and graphing were conducted using GraphPad Prism version 9 software (GraphPad Software, Inc.) and $p \leq 0.05$ was set for statistical significance.

## Results

### Animal characteristics and stress response

At the completion of the study, no significant differences were noted in body mass among group's (Table 1). Plasma levels of corticosterone were significantly 100% higher in the UCMS group compared to controls ($p < 0.05$). Behavioral assessments revealed poorer coat status of mice undergoing UCMS as well

**Table 1.** Animal characteristics.

| | Con | UCMS | Con+Feb | UCMS + Feb |
|---|---|---|---|---|
| Body Mass, g | 26.5 ± 4.2 | 24.8 ± 3.6 | 25.7 ± 3.5 | 26.2 ± 3.7 |
| Mean Blood Pressure, mmHg | 122 ± 11 | 127 ± 11 | 118 ± 12 | 129 ± 9 |
| Corticosterone, ng/ml | 112.5 ± 74.9 | 227.0 ± 126.4* | 150.0 ± 102.1 | 142.2 ± 67.7 |
| Coat Scores, AU | 0.5 ± 1.2 | 6.3 ± 1.3* | 0.9 ± 1.4 | 5.7 ± 1.8* |
| Sucrose Splash-Latency (sec) | 7.3 ± 7.2 | 20.5 ± 16.5* | 9.0 ± 8.0 | 24.3 ± 27.5* |
| Sucrose Splash-Number of Licks | 41.9 ± 20.7 | 27.5 ± 17.5* | 40.8 ± 17.3 | 25.1 ± 19.4* |

UCMS: unpredictable chronic mild stress. Mean ± SD. *$p < 0.05$ vs. Con; n = 22–28/group except corticosterone n = 11–12/group. 2 way ANOVA was performed.

as an increased latency to lick and a decreased number of licks in the sucrose splash test compared to control mice ($p < 0.05$) (Table 1). With the exception of corticosterone, all other stress behaviors remained elevated in the UCMS + Feb group compared to the control group (Table 1).

### *MCA function*

The endothelium-dependent dilation (EDD) of the MCA in response to increasing concentrations of ACh is summarized in Figure 1. Maximum EDD (at ACh $10^4$ log M) was 58% lower ($p < 0.001$) in UCMS compared to control mice (Figure 1(a)). This impaired EDD response was a result of a reduced NO-mediated dilation as indicated by a smaller reduction in EDD in the presence of the NO inhibitor L-NAME in the UCMS vs. the Con group ($4.3 \pm 1.8\,\mu m$ vs. $15.4 \pm 2.0\,\mu m$, $p < 0.001$) (Figure 1(b)). Next, we examined the effects of chronic febuxostat treatment on MCA function. Chronic febuxostat treatment prevented the impaired EDD to ACh with UCMS by restoring NO-mediated dilation (Figures 1(a) and (b)). There were no differences in NO-mediated EDD among the control, Con + Feb, and UCMS+Feb treated mice. Next, we examined the EID response of the MCA in response to increasing concentrations of SNP. No differences were noted among groups in the SNP dose-response or the maximal EID (at SNP$10^4$ log M) (Figure 1(c)). Similarly, the response of the MCA to PE, a potent vasoconstrictor, was also similar and was not affected by UCMS (Figure 1(d)). Further, the MCA response to SNP or PE was not affected by febuxostat.

To explore the role of oxidant-mediated impairment of MCA function, we acutely incubated the MCA with XO to induce a pro-oxidative environment, this XO incubation reduced ($p < 0.05$) maximal EDD in the Con and UCMS groups (Figure 2(a)). Next, we acutely incubated the MCA with Tempol (a SOD mimic) or febuxostat (XO inhibitor) (Figures 2(b) and (c)). Both reducers of oxidant levels were equally as effective

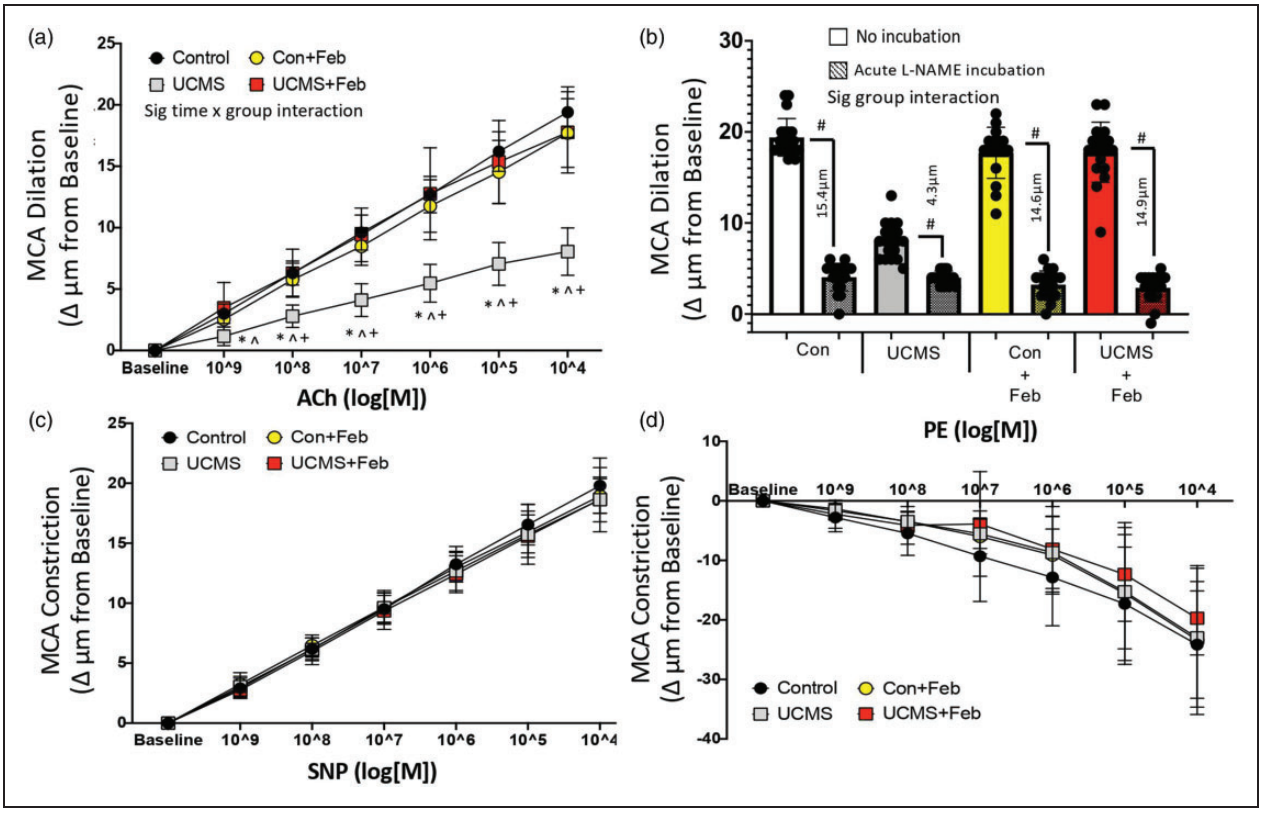


**Figure 1.** Cerebrovascular dilation. Middle cerebral artery (MCA) (a) dose-response curve for endothelial-dependent dilation (EDD) to acetylcholine (ACh), (b) maximal response of the MCA to the acetylcholine (ACh; $10^{-4}$ M) with and without the acute (30 min) incubation of L-NAME, the µm change values reflect the nitric oxide (NO)-dependent dilation = (Max $Dilation_{ACh}$) − (Max $Dilation_{ACh+L\text{-}NAME}$), (c) MCA dose-response curve for endothelial-independent dilation (EID) to sodium nitroprusside (SNP), and (e) the vasoconstrictor response to phenylephrine (PE) in control and UCMS mice with (+Feb) or without chronic febuxostat treatment. *$p < 0.05$ vs control; ^$p < 0.05$ vs control + Feb; $^{+}p < 0.05$ vs UCMS + Feb; $^{\#}p < 0.05$ vs no incubation experiment within the same group. mean ± SD. n = 16–20 mouse MCA's/group. Repeated measured ANOVA with a group-by-time interaction was performed and when a significant interaction (panel A and B only) was established a tukey post-hoc test was explored.

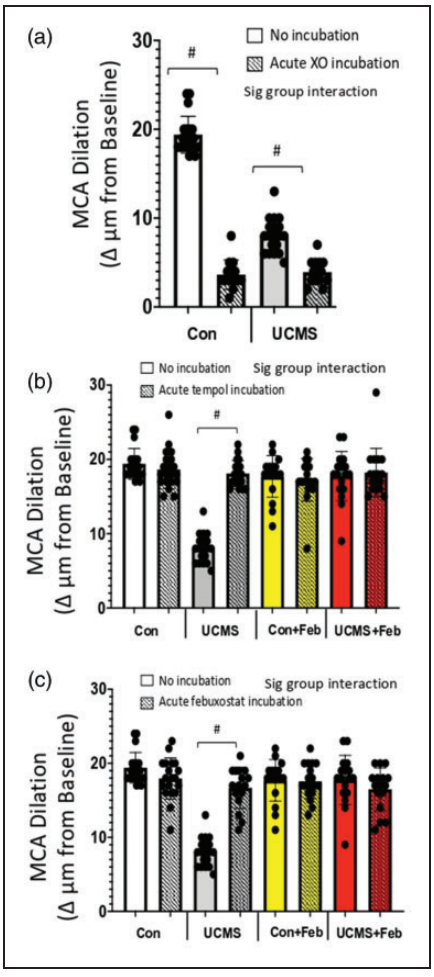


**Figure 2.** Maximal endothelial-dependent response and the role of oxidative stress. Maximal endothelial-dependent dilation to acetylcholine (ACh; $10^{-4}$M) during acute (30 min) incubation with xanthine oxidase (a), Tempol (b), and febuxostat (c). $^{\#}p < 0.05$ vs no incubation experiment within the same group; mean ± SD; n = 16–20 mouse MCA's/group. Repeated measured ANOVA with a group-by-incubation interaction was performed and when a significant interaction (all panels) was established a tukey post-hoc test was explored.

in restoring maximal EDD of the MCA in the UCMS group. Acute tempol and febuxostat incubation had no additional benefit on the maximal MCA EDD in the Con, Con + Feb, or UCMS + Feb groups.

### *MCA wall diameters and stiffness*

We examined the extent to which UCMS affected the structural phenotype of the MCA. MCA internal wall diameter did not differ among Con (93 ± 10µm), UCMS (90 ± 11 µm), Con+Feb (92 ± 11µm), or UCMS+Feb (91 ± 15 µm) group's. Similarly, wall thickness was not significantly different among Con (14 ± 3 µm), UCMS (14 ± 3 µm), Con + Feb (14 ± 4 µm), or UCMS + Feb (14 ± 4 µm) group's. Further, no significant differences were noted in percentage myogenic tone among groups (Con 36 ± 10%; UCMS 27 ± 11%; Con + Feb 40 ± 11%; UCMS + Feb 37 ± 12%).

### *Oxidative stress*

We used immuno-spin trapping, via western blot, to assess biomolecular free radical formation occurring under chronic stress conditions and the role of inhibiting XO. Densitometric analysis of the total staining for the entire lane (normalized to GAPDH), revealed 26% greater liver DMPO levels in the UCMS compared to controls ($p < 0.05$; Figure 3(a) and (b)). Whereas, liver DMPO concentrations were similar between Con and UCMS+Feb groups and significantly lower compared to the UCMS group (Figure 3(a) and (b)). To begin to understand the source of this increased free radical formation, XOR protein concentrations were examined in the liver. Chronic stress increased liver XOR concentrations by 87% ($p < 0.05$) compared to control mice (Figure 3(c) and (d)), which remained increased in the UCMS + Feb mice compared to controls. Next, we examined liver XO activity; however, no differences were noted in liver XO activity between the control and UCMS groups (Figure 3(e)). In contrast, Con + Feb and UCMS + Feb groups demonstrated diminished liver XO activity compared to the control and UCMS groups ($p < 0.05$, Figure 3(e)). As hydrogen peroxide is the main oxidant product of XO,[37] we used the coumarin boronic acid (CBA) assay to measure liver hydrogen peroxide production. Liver hydrogen peroxide production was 6-fold higher in the UCMS vs. control groups, whereas the UCMS + Feb group had similar levels of hydrogen peroxide in the liver compared to control mice (Figure 3(f)). In addition, we measured XO activity in the plasma (Figure 4) and found a 44% increase ($p < 0.05$) in XO activity in the UCMS compared to the control group, whereas plasma XO activity was significantly reduced in the UCMS + Feb group compared to the UCMS group.

Next, we explored the XO pathway in the brain. In brain homogenate, DMPO concentrations were similar among groups (Figure 5(a)). We then explored XOR protein levels and found similar concentrations of XOR among groups (Figure 5(b)). Similarly, XO activity in brain homogenate was similar among groups (Figure 5(c)). Next, we assessed hydrogen peroxide production within the brain homogenate and found a 5-fold increase in hydrogen peroxide production in the UCMS group compared to controls ($p < 0.05$; Figure 5 (d)). We also explored hydrogen peroxide concentrations in isolated brain microvessels and found a 2-fold increase in hydrogen peroxide production in the UCMS group compared to controls ($p < 0.05$;

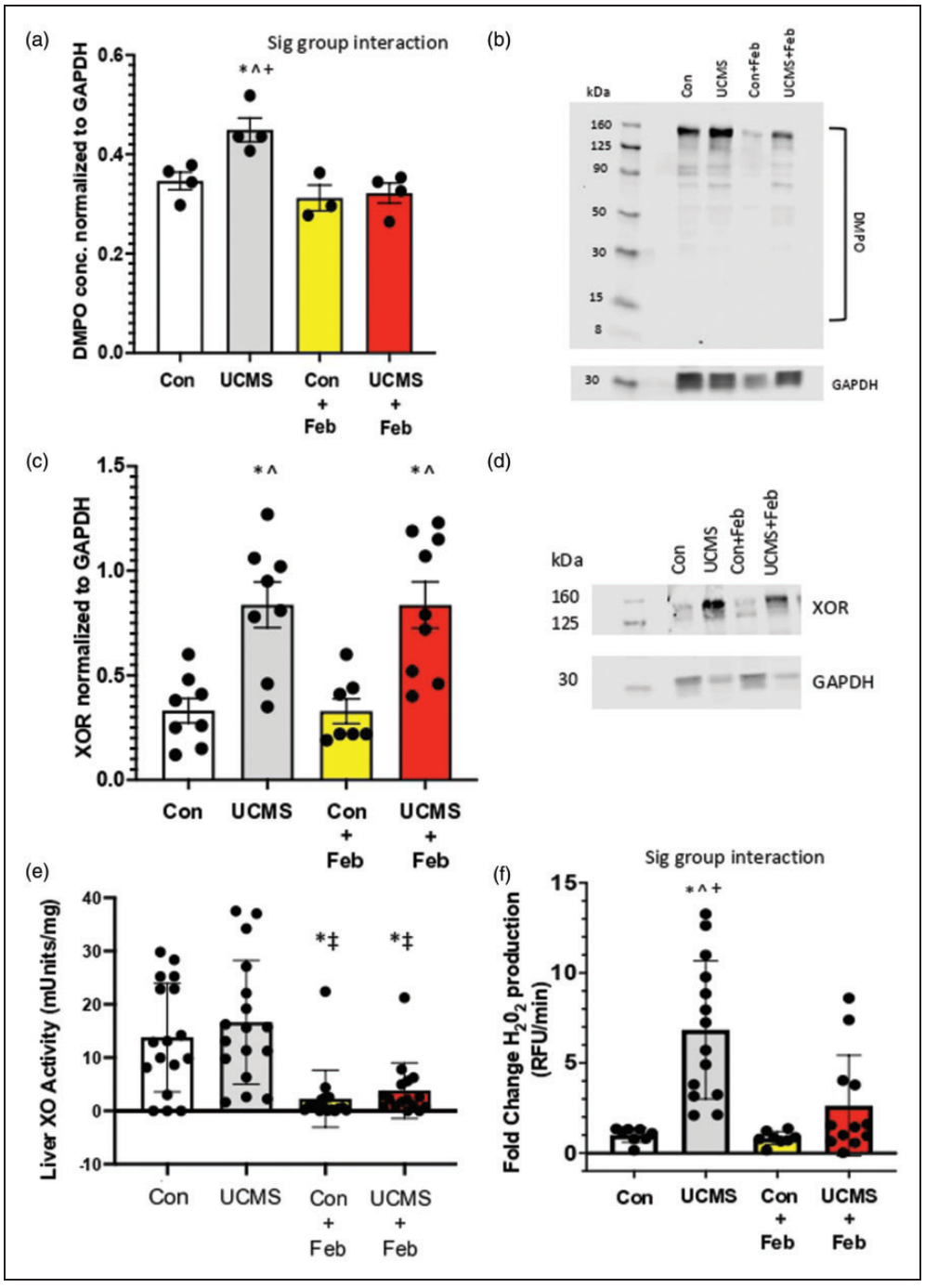


**Figure 3.** Oxidative stress in the liver. (a) 5,5-Dimethyl-1-Pyrroline-N-Oxide (DMPO) was used to detect free radical formation on biomolecules in the liver via western blotting; (b) quantification of DMPO western blot. (c) Xanthine oxidase reductase (XOR) expression was assessed within the liver using western blotting techniques; (d) quantification of XOR western blot. (e) Liver XO activity was measured with HPLC. (f) Liver hydrogen peroxide ($H_2O_2$) production using CBA assay. *$p < 0.05$ vs control; ^$p < 0.05$ vs control + Feb; ‡$p < 0.05$ vs. UCMS; $^{+}p < 0.05$ vs UCMS + Feb; Mean ± SD. n = 4–17 mouse samples/group. Two-way ANOVA with a group-by-drug interaction was performed and when a significant interaction (panel A and F) was established a tukey post-hoc test was explored, otherwise, the main variable effect was reported.

Figure 5(e)). Febuxostat prevented this increase in hydrogen peroxide production in both the brain and isolated brain microvessels ($p < 0.05$; Figures 5(d) and (e)).

### *Behavior*

Open field test was used as a measure of locomotive behaviors; no differences were noted in the total

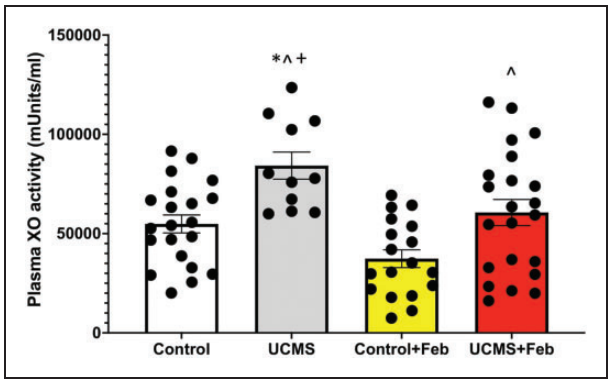


**Figure 4.** Plasma XO activity. Plasma XO activity was measured with HPLC. *$p < 0.05$ vs control; ^$p < 0.05$ vs control + Feb; $^{+}p < 0.05$ vs UCMS + Feb; mean ± SD. n = 12–23 mouse plasma samples/group. Two-way ANOVA with a group-by-drug interaction was performed, however, no significant interaction was established thus the main variable effect was reported.

number of beam breaks (Figure 6(a)) or the number of vertical beam breaks (rearing) (Figure 6(b)) among groups. Working memory was examined using the spontaneous alternation Y-maze, and we found that the UCMS mice were significantly ($p < 0.05$) impaired (18% reduction) in their ability to successfully undergo spontaneous alternation compared to control mice (Figure 6(e)). However, in contrast, the UCMS+Feb mice had a similar ability to successfully undergo spontaneous alternation compared to the control mice. Importantly, as noted with the open field test, and now with the y-maze test, the total distance traveled and the average speed was similar among groups (Figure 6(c) and (d)), indicating the potential confounding impact of locomotor disruptions on the cognitive effects was not evident.

## Discussion

The current study was undertaken to examine the role of XO in mediating chronic stress-induced cerebrovascular dysfunction. To accomplish our goal, we pharmacologically inhibited XO with febuxostat that was supplemented in the drinking water of chronically stressed mice. Cell culture work has shown that febuxostat (25 and 50 nM) was effective at reducing cell-bound oxidative stress production by 96 and 100%, respectively.[38] A number of novel observations were made in the current study: 1) chronic stress increased liver XOR production, and liver free radical formation including the increased production of $H_2O_2$, with an increase in circulating XO; 2) chronic stress increased the production of $H_2O_2$ in brain tissue and specifically within the cerebrovasculature; 3) febuxostat treatment during chronic stress prevented the stress-induced MCA EDD dysfunction by maintaining NO-dependent dilation; 4), febuxostat treatment prevented the increase in oxidative stress in the liver, brain, and cerebrovasculature, and lowered circulating XO; and lastly 5) the memory deficits noted with chronic stress were absent in the febuxostat treated mice. Thus, these data support the central hypothesis that XO plays an important role in the cerebrovascular dysfunction noted with chronic stress.

A previous study, using a more extreme form of stress (restraint stress) over 2 weeks compared to our progressive set of mild stresses that gradually build to induce a chronic stress-like phenotype over 8 weeks, increased XOR and XO activity, along with an accumulation of oxidative stress in visceral adipose tissue, liver, and intestines, and that treatment with febuxostat, suppressed stress-induced oxidative stress production.[11] Oxidative stress is a driving force for arterial dysfunction noted with chronic stress,[7,8,39] and our past work using a rat model has shown that oxidative stress plays a key role in the stress-induced MCA dysfunction as: 1) the oxidative load in the MCA of male UCMS rats was 2-fold higher vs. controls;[7] and 2) acute inhibition of oxidative stress with tempol rescued MCA function in male UCMS rats.[7] In the current study, we confirm in a mouse model, which includes both male and female mice, that chronic stress induces considerable cerebrovascular dysfunction alongside a pro-oxidative stress environment. A novel aspect of our study is the identification that XO plays a critical role in stress-induced cerebrovascular dysfunction. XOR includes the XO and XDH forms of the same enzyme. XOR is transcribed and translated from a single gene (*Xdh*) as XDH, which oxidizes hypoxanthine to xanthine to uric acid while reducing NAD+ to NADH. Under inflammatory or hypoxia conditions, XDH is post-translationally modified to XO which catalyzes the same purine reactions but uses oxygen as the electron acceptor to generate superoxide ($O_2^-$) and $H_2O_2$. The liver is one of the sites of greatest XOR activity and is the main source of circulating XOR.[21,40] When released from the hepatocytes into the circulation, XDH is rapidly converted to XO by plasma proteases and subsequently binds with high affinity to the endothelial GAGs,[19] where it can induce endothelial damage. In addition, the endothelium is also a source of XOR activity,[41] and we have shown XO-GAG interaction serves to amplify the local endothelial XOR levels in vascular beds distal from the site of origin (e.g. liver).[42,43]

To assess XO as a potential source of this oxidative stress environment, control (non-stressed mice) MCAs were incubated with XO and xanthine; these vessels displayed impaired MCA response to ACh, similar to the MCA dysfunction noted in UCMS mice. Further, acute incubation of the MCA from UCMS mice with

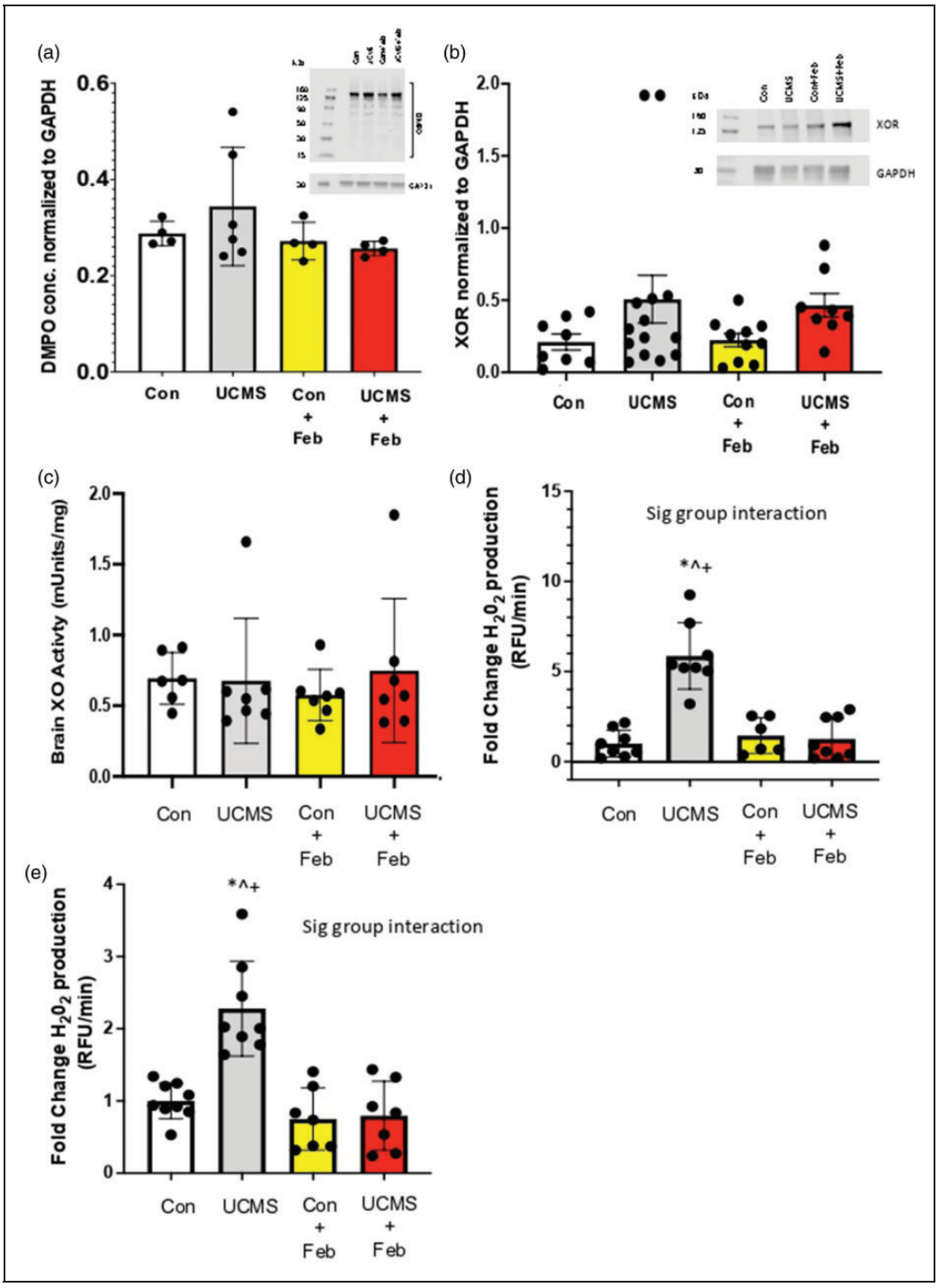


**Figure 5.** Oxidative stress in the brain and cerebrovasculature. (a) 5,5-Dimethyl-1-Pyrroline-N-Oxide (DMPO) was used to detect free radical formation on biomolecules in the brain via western blotting; (b) Xanthine oxidase reductase (XOR) concentration was assessed within the liver using western blotting techniques; (c) Brain XO activity was measured with HPLC; Hydrogen peroxide ($H_2O_2$) production was measured in whole brain homogenate (d) and isolated brain microvessels (e) musing the CBA assay. *$p < 0.05$ vs control; ^$p < 0.05$ vs control + Feb; $^{\ddagger}p < 0.05$ vs. UCMS; $^{+}p < 0.05$ vs UCMS + Feb; Mean ± SD. n = 4–14 mouse tissue samples/group. Two-way ANOVA with a group-by-drug interaction was performed and when a significant interaction (panel D and E) was established a tukey post-hoc test was explored, otherwise, the main variable effect was reported.

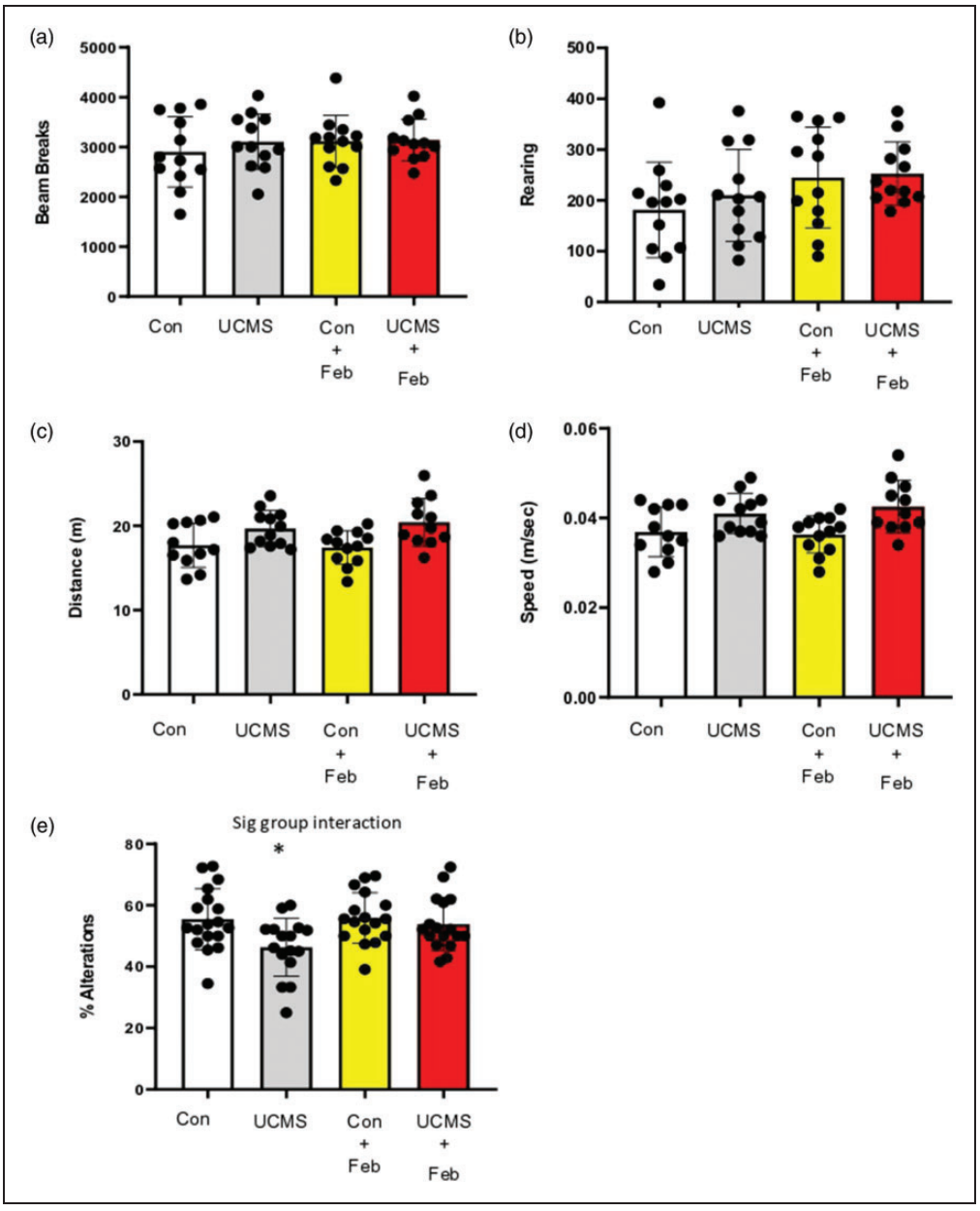


**Figure 6.** Locomotor and cognitive behavior with chronic stress. Open field test was used to measure locomotor behavior with total horizontal movements via beam breaks (fine and ambulatory combined) in the arena (a), and the number of vertical beam breaks (rearing; b). Spontaneous alternation Y-maze test was used to measure locomotor behavior (distance moved [C] and speed [D]) and working memory (e). Mean ± SD. n = 11–18 mice/group. *$p \leq 0.05$ vs control. Two-way ANOVA with a group-by-drug interaction was performed and when a significant interaction (panel e) was established a tukey post-hoc test was explored.

febuxostat rescued MCA EDD to ACh. In support of this, our chronic inhibition of XO with febuxostat (supplementation in the daily drinking water) of mice exposed to chronic stress prevented the dysfunction of the MCA. In particular, chronic febuxostat supplementation rescued the NO-dependent dilation in the pursuit of preserving endothelial function, potentially via two possible mechanisms. The first is that chronic stress inhibits endothelial NO synthase activity and prevents NO from being produced. This is supported in a model of aging, in that an inverse relationship was shown between XO expression and endothelial NO synthase with XO being named as the main contributor to the oxidative stress within the aorta.[44] It is also possible that chronic stress does not inhibit endothelial NO synthase activity, but instead invokes endothelial NO

synthase uncoupling resulting in peroxynitrite production and decreased NO bioavailability within the cerebrovasculature.[45,46]

It is important to note that no differences were noted in smooth muscle cell function either in the response of the MCA to SNP or the myogenic tone response. This is confirmed in past work in which healthy animals with no other predispositions exposed to chronic stress resulted in no smooth muscle cell dysfunction.[7] However, in instances of chronic stress predisposed with another comorbidity (i.e. obesity), smooth muscle cell dysfunction is present, both in SNP dilation and myogenic tone.[7] Importantly, obesity is associated with a substantial increase in the XO pathway[21] and we have shown that with obesity there is a substantial increase in vascular oxidative stress.[7] Further, inhibiting XO with febuxostat in the context of obesity prevented the increased liver production of XO and free radicals.[21] Interestingly, within the smooth muscle cells, uric acid and XO are capable of inducing inflammation and $O_2^-$ and peroxynitrite can blunt G protein-mediated activity and inhibit soluble guanylyl cyclase, respectively.[47–49]

The precise mechanism whereby chronic stress stimulates increased oxidative products leading to arterial dysfunction by XO is not entirely clear. XOR can increase oxidative stress via changes in the expression or activity of the enzyme. Our data shows that the XOR protein levels were significantly higher in the liver of UCMS mice, however, XO activity in the liver was similar between UCMS and control mice. This increased expression of XOR in the liver with stress coincides with an increased oxidative environment in the liver. We used an *in vivo* immuno-spin trapping method for indirectly assessing oxidant levels by detecting free radicals resulting from the reaction of oxidants with biomolecules to form stable, immunologically detectable nitrone-biomolecular adducts. We found that DMPO-labeled adducts were significantly elevated in the liver of UCMS mice compared to controls. This increased total free radical production in the liver was further supported by a significant increase in liver $H_2O_2$ production. Often, XO is mainly referred to as a source of $O_2^-$ with rare mention of the XO-catalyzed $H_2O_2$ production, and it is often assumed that $H_2O_2$ formation results from either reaction of XO-derived $O_2^-$ with superoxide dismutase or spontaneous dismutation of $O_2^-$. However, XO is a $H_2O_2$ producing enzyme that also produces some $O_2^-$.[42] Chronic febuxostat treatment with UCMS significantly reduced XO activity in the liver, however, XOR protein levels in the liver remained high. This is not surprising given that febuxostat does not impact XOR expression, but febuxostat does impact activity, as confirmed in our study, in both the Con+Feb and UCMS+Feb groups. In addition, we found a significant reduction in DMPO and $H_2O_2$ levels in the liver in the UCMS mice treated with febuxostat. These data would suggest that, in part, XO production in the liver with chronic stress is playing a significant role in the cerebrovascular dysfunction noted with chronic stress.

Liver XOR has been implicated in the facilitation of XO to the circulation resulting in its distribution to alternative tissue sites (like the brain vasculature), resulting in arterial dysfunction. Indeed, UCMS increased circulating XO which was lowered when UCMS was combined with chronic febuxostat treatments. Other sources of XOR may be equally important. Given the proximately of the brain tissue with the cerebrovasculature we explored XOR protein and XO activity in brain homogenate. No differences were noted in XOR protein or XO activity in the brain. However, $H_2O_2$ was significantly increased in the brain tissue of UCMS mice, and significantly reduced in the UCMS + Feb treated mice. Other studies have found that XOR expression and activity in brains were low compared to the liver[50] but the Xdh expression was upregulated with global brain ischemic reperfusion injury.[51] These data would suggest that the distribution of XOR in the brain is low, and perhaps not the source of XOR. However, further investigation is needed with genetic XOR knockout models. Importantly, we found that the production of $H_2O_2$ was 2-fold higher in the cerebrovasculature of UCMS compared to control mice, and that chronic febuxostat treatment with UCMS significantly reduced $H_2O_2$ production specifically in the cerebrovasculature. We were unable to measure total free radical production (using DMPO) in the cerebrovasculature due to low levels of protein. These data, along with the protection of the cerebrovascular function with chronic febuxostat treatment (ex vivo MCA data), would suggest that XO is playing a significant role in the cerebrovasculature. Indeed, the endothelial cells are an alternative source of XO, which may be responsible for the cerebrovascular dysfunction noted with stress and its protection with chronic febuxostat treatment. The presence and activity of XOR in endothelial cells have been noted by numerous studies.[52,53] Cultured endothelial cells exposed to hypoxia resulted in increased expression elevated protein abundance and enhanced enzymatic activity and extracellular release of XO.[54] Further, in humans, the levels of endothelial-bound XO correlate with the presence of coronary artery disease and are inversely proportional to flow-mediated brachial artery vasodilatation.[55] This XO-GAG association induces substantial sequestration and thus amplification of local endothelial XO concentration, producing a microenvironment primed for enhanced oxidative stress (i.e., a further shift in oxidant formation from $O_2^-$ to $H_2O_2$).[43] Thus, we have an

environment in which circulating XO can bind to the GAG on the endothelial cells (GAG-bound) to upregulate ROS generation, and this is further compounded by the local XO production from the endothelium (i.e., endothelial cell-bound XO). This deleterious action of XO has been noted in various reports of arterial and cardiopulmonary diseases including heart failure, pulmonary hypertension, sickle cell disease, and diabetes.[56–59]

The potential clinical consequences of chronic stress on brain health are evident in the reduction in working memory in chronically stressed mice, as assessed by the y-maze test. These data suggesting that chronic stressful events can lead to cognitive decline are supported in both human,[60,61] and animal models.[62,63] Epidemiological data indicate that stressed individuals are more likely to develop mild cognitive impairment, or even dementia, compared to non-stressed individuals.[64,65] Working memory is perhaps one of the most well-modeled aspects of the cognitive deficits in Alzheimer's Disease,[66] and the Y-maze type tasks, which require spatial working memory to solve, are one of the most widely used paradigms for working memory in mice. Epidemiological,[67–71] and pre-clinical studies[72–74] support the idea that arterial alterations are early events in cognitive deficits and one of the strongest brain pathology associated with Alzheimer's Disease. As such, the cerebrovascular dysfunction noted with chronic stress, coupled with the increased oxidative environment in the brain and cerebrovasculature is a possible mechanistic pathway linking chronic stress and cognitive decline. Indeed, we show that blocking XO with febuxostat not only protected the cerebrovascular function but also prevented the decline in working memory that was noted with chronic stress. The relationship between chronic stress and cognitive decline is particularly important for the health of older adults who are at greater risk for developing dementia. There is a known link between age-associated oxidative stress leading to cerebrovascular dysfunction and cognitive decline.[71,75] And along the lines of the two-hit vascular hypothesis of Alzheimer's Disease, the compromised health of the cerebrovasculature with chronic stress, maybe an initial insult that is sufficient to initiate neural injury and neurodegeneration, and promote the accumulation of amyloid β-peptide and tau accumulation and phosphorylation. In fact, animal studies have shown a link between stress and neuropathology associated with dementia, demonstrating that stress is associated with synapse loss,[76] increases in amyloid β-peptide,[77,78] and tau accumulation and phosphorylation.[78,79]

## Conclusions

The present study demonstrates the role of XO in chronic stress-induced cerebrovascular dysfunction. We show that chronic stress increased liver XO production as well as increased free radical formation within the liver, brain, and cerebrovasculature. Chronic febuxostat supplementation prevented the stress-induced MCA dysfunction, prevented the stress-induced pro-oxidative stress environment within the liver, brain, and cerebrovasculature, and prevented stress-induced deficits in working memory. Taken together, these data support the role of XO in chronic stress-induced cerebrovascular dysfunction.

### Funding

The author(s) disclosed receipt of the following financial support for the research, authorship, and/or publication of this article: This study was supported by the National Institute of Neurological Disorders and Stroke (PDC: R01NS117754); National Institute of General Medical Sciences of the National Institutes of Health (PDC and EEK; U54GM104942, and 5P20GM109098); National Institute of Aging (EB: T32 AG052375).

### Declaration of conflicting interests

The author(s) declared no potential conflicts of interest with respect to the research, authorship, and/or publication of this article.

### Authors' contributions

The study was performed in PDC and EE laboratories. PDC, EB, SP, RC, ED, RWB, EE: Conceptualized and designed the study; PDC, EB, EE; undertook experiments and analyzed data; EB, ED, EE; All authors critically reviewed the manuscript and approved the final manuscript as submitted and agree to be accountable for all aspects of the work.

### ORCID iD

Paul D Chantler https://orcid.org/0000-0001-6960-9728

### References

1. Collaborators C-MD. Global prevalence and burden of depressive and anxiety disorders in 204 countries and territories in 2020 due to the COVID-19 pandemic. *Lancet* 2021; 398: 1700–1712.
2. Joëls M and Baram TZ. The neuro-symphony of stress. *Nat Rev Neurosci* 2009; 10: 459–466.
3. Anderson NB, Belar CD, Breckler SJ, et al. *Stress in America: paying with our health*. Washington DC, USA: American Psychological Association, 2015.
4. Booth J, Connelly L, Lawrence M, et al. Evidence of perceived psychosocial stress as a risk factor for stroke in adults: a meta-analysis. *BMC Neurol* 2015; 15: 233.
5. Bisht K, Sharma K and Tremblay ME. Chronic stress as a risk factor for Alzheimer's disease: roles of microglia-mediated synaptic remodeling, inflammation, and oxidative stress. *Neurobiol Stress* 2018; 9: 9–21.

6. Tong X, Yang Q, Ritchey MD, et al. The burden of cerebrovascular disease in the United States. *Prev Chronic Dis* 2019; 16: E52.
7. Brooks S, Branyan KW, DeVallance E, et al. Psychological stress-induced cerebrovascular dysfunction: the role of metabolic syndrome and exercise. *Exp Physiol* 2018; 103: 761–776.
8. Chantler P, Shrader CD, Tabone LE, et al. Cerebral cortical microvascular rarefaction in metabolic syndrome is dependent on insulin resistance and loss of nitric oxide bioavailability. *Microcirculation* 2015; 22: 435–445.
9. Michel TM, Camara S, Tatschner T, et al. Increased xanthine oxidase in the thalamus and putamen in depression. *World J Biol Psychiatry* 2010; 11: 314–320.
10. Herken H, Gurel A, Selek S, et al. Adenosine deaminase, nitric oxide, superoxide dismutase, and xanthine oxidase in patients with major depression: impact of antidepressant treatment. *Arch Med Res* 2007; 38: 247–252.
11. Yisireyili M, Hayashi M, Wu H, et al. Xanthine oxidase inhibition by febuxostat attenuates stress-induced hyperuricemia, glucose dysmetabolism, and prothrombotic state in mice. *Sci Rep* 2017; 7: 1266.
12. Shirakura T, Nomura J, Matsui C, et al. Febuxostat, a novel xanthine oxidoreductase inhibitor, improves hypertension and endothelial dysfunction in spontaneously hypertensive rats. *Naunyn Schmiedebergs Arch Pharmacol* 2016; 389: 831–838.
13. Schmidt HM, Wood KC, Lewis SE, et al. Xanthine oxidase drives hemolysis and vascular malfunction in sickle cell disease. *Arterioscler Thromb Vasc Biol* 2021; 41: 769–782.
14. Itano S, Kadoya H, Satoh M, et al. Non-purine selective xanthine oxidase inhibitor ameliorates glomerular endothelial injury in $Ins^{Akita}$ diabetic mice. *Am J Physiol Renal Physiol* 2020; 319: F765–F772.
15. Schmidt HM, Kelley EE and Straub AC. The impact of xanthine oxidase (XO) on hemolytic diseases. *Redox Biol* 2019; 21: 101072.
16. Boueiz A, Damarla M and Hassoun PM. Xanthine oxidoreductase in respiratory and cardiovascular disorders. *Am J Physiol Lung Cell Mol Physiol* 2008; 294: L830–40.
17. Tan S, Yokoyama Y, Dickens E, et al. Xanthine oxidase activity in the circulation of rats following hemorrhagic shock. *Free Radic Biol Med* 1993; 15: 407–414.
18. Pritsos CA. Cellular distribution, metabolism and regulation of the xanthine oxidoreductase enzyme system. *Chem Biol Interact* 2000; 129: 195–208.
19. Houston M, Estevez A, Chumley P, et al. Binding of xanthine oxidase to vascular endothelium. Kinetic characterization and oxidative impairment of nitric oxide-dependent signaling. *J Biol Chem* 1999; 274: 4985–4994.
20. Percie Du Sert N, Hurst V, Ahluwalia A, et al. The ARRIVE guidelines 2.0: updated guidelines for reporting animal research. *J Cereb Blood Flow Metab* 2020; 40: 1769–1777.
21. Harmon DB, Mandler WK, Sipula IJ, et al. Hepatocyte-specific ablation or whole-body inhibition of xanthine oxidoreductase in mice corrects obesity-induced systemic hyperuricemia without improving metabolic abnormalities. *Diabetes* 2019; 68: 1221–1229.
22. Mineur YS, Belzung C and Crusio WE. Effects of unpredictable chronic mild stress on anxiety and depression-like behavior in mice. *Behav Brain Res* 2006; 175: 43–50.
23. Willner P. The chronic mild stress (CMS) model of depression: history, evaluation and usage. *Neurobiol Stress* 2017; 6: 78–93.
24. Branyan KW, Devallance ER, Lemaster KA, et al. Role of chronic stress and exercise on microvascular function in metabolic syndrome. *Med Sci Sports Exerc* 2018; 50: 957–966.
25. Stanley SC, Brooks SD, Butcher JT, et al. Protective effect of sex on chronic stress- and depressive behavior-induced vascular dysfunction in BALB/cJ mice. *J Appl Physiol (1985)* 2014; 117: 959–970.
26. DeVallance ER, Branyan KW, Olfert IM, et al. Chronic stress induced perivascular adipose tissue impairment of aortic function and the therapeutic effect of exercise. *Exp Physiol* 2021; 106: 1343–1358.
27. Yalcin I, Aksu F and Belzung C. Effects of desipramine and tramadol in a chronic mild stress model in mice are altered by yohimbine but not by pindolol. *Eur J Pharmacol* 2005; 514: 165–174.
28. Frisbee JC, Brooks SD, Stanley SC, et al. An unpredictable chronic mild stress protocol for instigating depressive symptoms, behavioral changes and negative health outcomes in rodents. *J Vis Exp* 2015; 106.
29. Denenberg VH. Open-field bheavior in the rat: what does it mean? *Ann N Y Acad Sci* 1969; 159: 852–859.
30. Harper SL, Bohlen HG and Rubin MJ. Arterial and microvascular contributions to cerebral cortical autoregulation in rats. *Am J Physiol* 1984; 246: H17–24.
31. Kelley EE, Batthyany CI, Hundley NJ, et al. Nitro-oleic acid, a novel and irreversible inhibitor of xanthine oxidoreductase. *J Biol Chem* 2008; 283: 36176–36184.
32. Austin SA and Katusic ZS. Partial loss of endothelial nitric oxide leads to increased cerebrovascular beta amyloid. *J Cereb Blood Flow Metab* 2020; 40: 392–403.
33. Zielonka J, Cheng G, Zielonka M, et al. High-throughput assays for superoxide and hydrogen peroxide: design of a screening workflow to identify inhibitors of NADPH oxidases. *J Biol Chem* 2014; 289: 16176–16189.
34. DeVallance E, Branyan KW, Lemaster KC, et al. Exercise training prevents the perivascular adipose tissue-induced aortic dysfunction with metabolic syndrome. *Redox Biol* 2019; 26: 101285.
35. Khoo NK, Cantu-Medellin N, Devlin JE, et al. Obesity-induced tissue free radical generation: an in vivo immuno-spin trapping study. *Free Radic Biol Med* 2012; 52: 2312–2319.
36. Khoo NKH, Cantu-Medellin N, S, Croix C, et al. In vivo immuno-spin trapping: imaging the footprints of oxidative stress. *Curr Protoc Cytom* 2015; 74: 12.42.1–12.4211.
37. Kelley EE, Khoo NK, Hundley NJ, et al. Hydrogen peroxide is the major oxidant product of xanthine oxidase. *Free Radic Biol Med* 2010; 48: 493–498.

38. Malik UZ, Hundley NJ, Romero G, et al. Febuxostat inhibition of endothelial-bound XO: implications for targeting vascular ROS production. *Free Radic Biol Med* 2011; 51: 179–184.
39. De Silva TM, Li Y, Kinzenbaw DA, et al. Endothelial PPARgamma (peroxisome proliferator-activated receptor-gamma) is essential for preventing endothelial dysfunction with aging. *Hypertension* 2018; 72: 227–234.
40. Parks DA and Granger DN. Xanthine oxidase: biochemistry, distribution and physiology. *Acta Physiol Scand Suppl* 1986; 548: 87–99.
41. Landmesser U, Spiekermann S, Preuss C, et al. Angiotensin II induces endothelial xanthine oxidase activation: role for endothelial dysfunction in patients with coronary disease. *Arterioscler Thromb Vasc Biol* 2007; 27: 943–948.
42. Kelley EE. Biochemistry of molybdopterin nitrate/nitrite reductases. *Nitric oxide: biology and pathobiology*. 3rd edition. London, UK: Academic Press (an imprint of Elsevier), 2017, pp.173–184.
43. Kelley EE, Trostchansky A, Rubbo H, et al. Binding of xanthine oxidase to glycosaminoglycans limits inhibition by oxypurinol. *J Biol Chem* 2004; 279: 37231–37234.
44. Newaz MA, Yousefipour Z and Oyekan A. Oxidative stress-associated vascular aging is xanthine oxidase-dependent but not NAD(P)H oxidase-dependent. *J Cardiovasc Pharmacol* 2006; 48: 88–94.
45. Guzik TJ, West NE, Pillai R, et al. Nitric oxide modulates superoxide release and peroxynitrite formation in human blood vessels. *Hypertension* 2002; 39: 1088–1094.
46. Santhanam AV, d'Uscio LV, He T, et al. Uncoupling of endothelial nitric oxide synthase in cerebral vasculature of Tg2576 mice. *J Neurochem* 2015; 134: 1129–1138.
47. Armstead WM. Protein kinase C activation generates superoxide and contributes to impairment of cerebrovasodilation induced by G protein activation after brain injury. *Brain Res* 2003; 971: 153–160.
48. Dai Y, Cao Y, Zhang Z, et al. Xanthine oxidase induces foam cell formation through LOX-1 and NLRP3 activation. *Cardiovasc Drugs Ther* 2017; 31: 19–27.
49. Weber M, Lauer N, Mulsch A, et al. The effect of peroxynitrite on the catalytic activity of soluble guanylyl cyclase. *Free Radic Biol Med* 2001; 31: 1360–1367.
50. Suzuki G, Okamoto K, Kusano T, et al. Evaluation of neuronal protective effects of xanthine oxidoreductase inhibitors on severe whole-brain ischemia in mouse model and analysis of xanthine oxidoreductase activity in the mouse brain. *Neurol Med Chir (Tokyo)* 2015; 55: 77–85.
51. Yamaguchi M, Okamoto K, Kusano T, et al. The effects of xanthine oxidoreductase inhibitors on oxidative stress markers following global brain ischemia reperfusion injury in C57BL/6 mice. *PLoS One* 2015; 10: e0133980.
52. Phan SH, Gannon DE, Varani J, et al. Xanthine oxidase activity in rat pulmonary artery endothelial cells and its alteration by activated neutrophils. *Am J Pathol* 1989; 134: 1201–1211.
53. Sohn HY, Krotz F, Gloe T, et al. Differential regulation of xanthine and NAD(P)H oxidase by hypoxia in human umbilical vein endothelial cells. Role of nitric oxide and adenosine. *Cardiovasc Res* 2003; 58: 638–646.
54. Kelley EE, Hock T, Khoo NK, et al. Moderate hypoxia induces xanthine oxidoreductase activity in arterial endothelial cells. *Free Radic Biol Med* 2006; 40: 952–959.
55. Landmesser U, Spiekermann S, Dikalov S, et al. Vascular oxidative stress and endothelial dysfunction in patients with chronic heart failure: role of xanthine-oxidase and extracellular superoxide dismutase. *Circulation* 2002; 106: 3073–3078.
56. Aslan M, Ryan TM, Adler B, et al. Oxygen radical inhibition of nitric oxide-dependent vascular function in sickle cell disease. *Proc Natl Acad Sci U S A* 2001; 98: 15215–15220.
57. Butler R, Morris AD, Belch JJ, et al. Allopurinol normalizes endothelial dysfunction in type 2 diabetics with mild hypertension. *Hypertension* 2000; 35: 746–751.
58. Desco MC, Asensi M, Marquez R, et al. Xanthine oxidase is involved in free radical production in type 1 diabetes: protection by allopurinol. *Diabetes* 2002; 51: 1118–1124.
59. Farquharson CA, Butler R, Hill A, et al. Allopurinol improves endothelial dysfunction in chronic heart failure. *Circulation* 2002; 106: 221–226.
60. Lupien SJ, de Leon M, de Santi S, et al. Cortisol levels during human aging predict hippocampal atrophy and memory deficits. *Nat Neurosci* 1998; 1: 69–73.
61. Peavy GM, Salmon DP, Jacobson MW, et al. Effects of chronic stress on memory decline in cognitively normal and mildly impaired older adults. *Am J Psychiatry* 2009; 166: 1384–1391.
62. Yuen EY, Wei J, Liu W, et al. Repeated stress causes cognitive impairment by suppressing glutamate receptor expression and function in prefrontal cortex. *Neuron* 2012; 73: 962–977.
63. Han B, Wang JH, Geng Y, et al. Chronic stress contributes to cognitive dysfunction and hippocampal metabolic abnormalities in APP/PS1 mice. *Cell Physiol Biochem* 2017; 41: 1766–1776.
64. Wilson RS, Evans DA, Bienias JL, et al. Proneness to psychological distress is associated with risk of Alzheimer's disease. *Neurology* 2003; 61: 1479–1485.
65. Wilson RS, Schneider JA, Boyle PA, et al. Chronic distress and incidence of mild cognitive impairment. *Neurology* 2007; 68: 2085–2092.
66. Roberts RO, Knopman DS, Mielke MM, et al. Higher risk of progression to dementia in mild cognitive impairment cases who revert to normal. *Neurology* 2014; 82: 317–325.
67. Gelber RP, Launer LJ and White LR. The Honolulu-Asia aging study: epidemiologic and neuropathologic research on cognitive impairment. *Curr Alzheimer Res* 2012; 9: 664–672.
68. Breteler MM, Claus JJ, Grobbee DE, et al. Cardiovascular disease and distribution of cognitive function in elderly people: the Rotterdam study. *BMJ* 1994; 308: 1604–1608.
69. Bennett DA, Buchman AS, Boyle PA, et al. Religious orders study and rush memory and aging project. *J Alzheimers Dis* 2018; 64: S161–S189.

70. Iturria-Medina Y, Sotero RC, Toussaint PJ, et al. Early role of vascular dysregulation on late-onset Alzheimer's disease based on multifactorial data-driven analysis. *Nat Commun* 2016; 7: 11934.
71. Montagne A, Barnes SR, Sweeney MD, et al. Blood-brain barrier breakdown in the aging human hippocampus. *Neuron* 2015; 85: 296–302.
72. Ngandu T, Lehtisalo J, Solomon A, et al. A 2 year multidomain intervention of diet, exercise, cognitive training, and vascular risk monitoring versus control to prevent cognitive decline in at-risk elderly people (FINGER): a randomised controlled trial. *Lancet* 2015; 385: 2255–2263.
73. Snowdon DA, Greiner LH, Mortimer JA, et al. Brain infarction and the clinical expression of Alzheimer disease. The nun study. *JAMA* 1997; 277: 813–817.
74. Richard T, Pawlus AD, Iglésias M-L, et al. Neuroprotective properties of resveratrol and derivatives. *Ann N Y Acad Sci* 2011; 1215: 103–108.
75. Camici GG, Savarese G, Akhmedov A, et al. Molecular mechanism of endothelial and vascular aging: implications for cardiovascular disease. *Eur Heart J* 2015; 36: 3392–3403.
76. Tata DA, Marciano VA and Anderson BJ. Synapse loss from chronically elevated glucocorticoids: relationship to neuropil volume and cell number in hippocampal area CA3. *J Comp Neurol* 2006; 498: 363–374.
77. Devi L, Alldred MJ, Ginsberg SD, et al. Sex- and brain region-specific acceleration of beta-amyloidogenesis following behavioral stress in a mouse model of Alzheimer's disease. *Mol Brain* 2010; 3: 34.
78. Jeong YH, Park CH, Yoo J, et al. Chronic stress accelerates learning and memory impairments and increases amyloid deposition in APPV717I-CT100 transgenic mice, an Alzheimer's disease model. *Faseb J* 2006; 20: 729–731.
79. Green KN, Billings LM, Roozendaal B, et al. Glucocorticoids increase amyloid-beta and tau pathology in a mouse model of Alzheimer's disease. *J Neurosci* 2006; 26: 9047–9056.